Scientific Research Publishing

The Alumina Film Nanomorphology Formed to Improve the Corrosion Resistance of Al-2.0 wt% Fe Alloy as Result of the Laser Surface Melting Technique Applied

Moises Meza Pariona, Katieli Tives Micene

Graduate Program in Engineering and Materials Science, State University of Ponta Grossa (UEPG), Ponta Grossa, Brazil
Email: mmpariona@uepg.br

Abstract

The laser surface remelting (LSR) treatment was performed to Al-2.0 wt% Fe alloy with a 2 kW Yb-fiber laser (IPG YLR-2000S). The substrate and laser-treated material characterization were executed using different techniques. Among them, the microstructure was analyzed by optical microscope, SEM, low-angle X-ray diffraction (LAXRD) and the corrosion test was made in aerated solution of 0.1 M H_2SO_4 at a temperature of 25°C ± 0.5°C. As result was shown, the micrograph of LSR-treated material displaying can be a fine cellular structure and the existence of certain nanoporosities and a similar to a nano-dendritic growth was observed too. The characteristic of melted zone was constituted of metastable phases according to the result of x-rays and the behavior corrosion as a result of the LSR-treated sample, which it was shown to be more resistant to corrosion than the untreated sample. A comparative study was carried out of the cyclic polarization of the laser-treated and untreated samples, demonstrating that the reduction and oxidation reverse peaks were not observed and being the cyclic polarization behavior was of irreversible character in both samples, however, the LSR-treated sample propitious the passivity on the surface also reduced the corrosion phenomena. Wherefore, this type of laser-treated alloy can be applied in the aerospace, aeronautic and automobilist industries.

Keywords

Al-2.0 wt% Fe Alloy, Laser-Treated, Microstructure, Low-Angle X-Ray Diffraction, Cyclical Polarization

1. Introduction

The aluminum oxide or alumina has important properties, because the alumina is produced during the laser surface remelting (LSR) treatment, and this technique does not

suit within the traditional techniques. It is a modern technique that is being used recently, therefore it is important to focus on this work. As well, the authors Nakajima *et al.* [1] studied the formation behavior of the anodic alumina nanofibers via constant voltage pyrophosphoric acid anodizing. They have discussed extensively on aluminum oxide films fabricated via anodizing in various electrolyte solutions. Furthermore, they affirm that this technique has been widely investigated in various applied sciences and technologies due to their characteristic nanomorphologies and chemical/physical properties. In general, anodic aluminum oxide can be classified into two different types, as follows: barrier and porous oxides. Barrier oxides have been widely used for electrolytic capacitor applications due to their high dielectric property. Anodic porous alumina has been widely used for various nanoapplications, such as optical devices and nanotemplates.

The laser surface treatment of metals is a process where a small surface volume of materials is melted instantly by a laser beam and cooled rapidly, thereby producing very fine microstructure with an improved wear and corrosion resistance. Laser surface melting (LSM) was reported by authors Lee *et al.* [2] to improve the corrosion resistance of Zircaloy-4 in acid solution.

In this study, the microstructural and corrosion resistance analysis of the hypereutectic Al-2.0 wt% Fe alloy LSR-treated was performed and this was the aim of this research, where the substrate and laser-treated material were characterized using different techniques. Among them, the microstructure was analyzed by optical microscope, SEM, low-angle X-ray diffraction (LAXRD) analysis and the corrosion test was performed in aerated solution of 0.1 M H_2SO_4 at a temperature of 25°C ± 0.5°C. In the electrochemical study, the following tests were carried out: open circuit potential, the polarization resistance, the corrosion current, determination of the corrosion rate and finally cyclical polarization for the untreated and laser-treated samples. The importance of this research is due that this LSR-treated alloy presented metastable phases, which between them, what are of greater importance are alumina and nitrite, the presence of a fine cellular structure and the existence of certain nano-porosities, a high corrosion resistance and a large plateau of passive zone, and therefore this type of laser-treated alloy can be applied in the aerospace, aeronautic and automobilist industries.

2. Materials and Methods

Experimental Characterization

Material

Al-2.0 wt% Fe alloy was prepared with commercially pure raw materials, being that the aluminum has 99.76% purity, containing 1.54 wt% of iron, and other elements with quantities below 50 PPM. The casting assembly used in solidification experiments consists of a water-cooled mold and the heat was extracted only from the bottom, promoting vertical upward directional solidification. This apparatus was used to obtain cylindrical casting, with dimensions of 6 cm diameter and 10 cm length. The preparation of samples for the analysis consisted in sectioning the cylindrical casting into several longitudinal slices, and milling the surfaces to improve parallelism. Each piece was sanded with 1200# SiC sand paper and then sand-blasted was applied to reduce the surface ref-

lectivity, thus increasing the laser energy absorption coefficient.

Laser Surface Remelting Treatment Specifications

The laser surface remelting (LSR) treatment was performed with a 2 kW Yb-fiber laser (IPG YLR-2000S) that operates at wavelength of 1.07 μm. The laser beam is coupled to a 160 mm focusing lens (optical head). For this optical system the focused beam diameter was 100 μm. The laser output power was 600 W and the scanning speed was 40 mm·s^{-1}. For this experiment, the sample was positioned 3 mm above the focus (out of focus), which results in a 600 μm diameter laser beam, which was designed by Riva *et al.* [3]. Assuming a near Gaussian laser beam profile, the power density was 21.2×10^4 W·cm^{-2}, which were studded by Steen and Mazumde [4]. The average distance between weld fillets was 300 μm. The device operated without shielding gas in order to increase between the metal and the ambient gas which contributes to the formation of a passivation oxide layer on the surface of the substrate.

After the laser processing, different regions were identified on the cross-section of the sample, through the SEM micrographs analysis: laser melted zone (LMZ), the interface between the treated region and the substrate, and unaffected region (substrate), which was studied by Pariona *et al.* [5]. On the surface of the sample there are two distinct regions: the region on weld fillet and the region between weld fillets, this has been discussed and studied by the authors Pariona *et al.* [5] [6].

Characterization Techniques

The substrate and laser-treated material characterization was performed using different techniques. Therefore, the microstructure was analyzed by a Shimadzu SSX-550 scanning electron microscope (SEM) and an Olympus BX-51 optical microscope (OM) with a QColor 3 digital camera for the image capture. The SEDS-500 energy dispersive spectroscopy (EDS) equipment was used for semi-quantitative analysis and it was coupled to SEM. As well, low-angle X-ray diffraction (LAXRD) analysis were recorded at a scan speed of 0.2˚min^{-1}, using a Lab XRD-6000 diffractometer (minimum detection >1%). The corrosion test was performed in aerated solution of 0.1 M H_2SO_4 at a temperature of 25˚C ± 0.5˚C. Working electrodes of surface-treated and untreated samples were prepared with epoxy resin to expose a top surface. Corrosion potentials (Ecor) were measured using Autolab PGSTAT 30 potentiostat system connected to a microcomputer. The samples were cut with diamond disk. For the cross-section analysis them were sanded (600 up to 1200 #), then polished with diamond paste (1 μm) and colloidal silica. The chemical attack with 0.5% HF was also made on these samples for analysis microscopic.

3. Results and Discussions

3.1. Study of the Electrochemical Behavior of the Samples

To better understand the corrosion process that occurs of the laser-treated Al-2.0 wt% Fe alloy, firstly a study of the micrographs of samples in both, as much on the surface and as well as on the cross-section were executed, the details of the changes that suffers when was subjected to RSL-treatment sample and whose results will be shown to follow. Soon it will be discussed the influence of micrograph on the result of the electrochemical study. As well, in the electrochemical study, the following tests were carried

out, among them, open circuit potential (OCP), the polarization resistance, the corrosion current (I_{cor}), determination of the corrosion rate and finally cyclical polarization for untreated and laser-treated samples.

3.2. Microstructural Study

In this work, all untreated surface of Al-2.0 wt% Fe alloy was covered with an arrangement of multiple weld fillets, in order to analyze this treatment. Micro-porosity has been observed on the surface of the laser-treated sample and more preferably in the region on the weld fillet. Besides that, the protuberance on this surface was observed, which corresponds to the region on the weld fillet, a similar result of this microstructure was given by authors Sun *et al.* [7].

Figure 1 shows the cross-section analysis of the specimen, where the three different regions are observed: the melted zone, the interface between the treated region and the substrate, and specifically the substrate.

The first region (Figure 1(a)) is characterized by a fine cellular structure, as well as, the existences of certain nano-porosities and also in this region the presence of protuberances is observed, which they corresponds to the region between weld fillets. According to the authors Pariona *et al.* [8], the presence of the protuberances is more perceptible in Al-1.5 wt% Fe alloy than Al-2.0 wt% Fe alloy. In Figure 1(a) it's observed, the overlapping lines and being more magnified in Figure 1(b), these highlighted lines are due to the overlapping of consecutive weld fillets, this phenomenon was also observed by the authors Yan *et al.* [9], they have verified, which the melt pools are overlapping one with other.

These overlapping lines are most notorious in Al-2.0 wt% Fe alloy that in Al-1.5 wt% Fe alloy [5] [6] [8]. Here it should be pointed, despite that the velocity of the laser beam was remained the same at 40 mm/s, for the treatment of the hypoeutectic Al-1.5 wt% Fe alloy and to the hypereutectic Al-2.0 wt% Fe alloy, because, the difference of the Fe concentration had significant influence on the characteristic of the overlapping lines, in the melted zone region. In order to clarity, the region of Figure 1(b) has been still more magnified as shown in Figure 1(c), where is observed a similar to a nano-dendritic growth, possibly following the direction of the thermal gradient and however, around the overlapping lines there are a high concentration of nano-porosity, that it can be noticed. However, in the region between the overlapping lines in Figure 1(d), with high magnification is observed a fine cellular structure with columnar growth, this result is similar to study realized by the authors Olakanmia *et al.* [10] and Fu *et al.* [11].

On the other hand, in the interface between the treated region and the substrate was not observed clearly the feature of the heat affected zone (HAZ), it has been studied by other authors, between them, Bertelly *et al.* [12], these authors have affirmed for low Fe concentration does not appear the HAZ. This region was magnified in Figure 1(e), which shown a structure with growth similar to nano-dendritic, following the direction of the thermal gradient to the substrate region. Specifically the substrate region of Al-2.0 wt% Fe alloy, the micrograph of this region is similar to Al-1.5 wt% Fe alloy, which is constituted by grain boundaries, as such has been studied by the authors Pariona *et al.* [8], these authors confirmed the matrix with second-phase particles, which precipi-
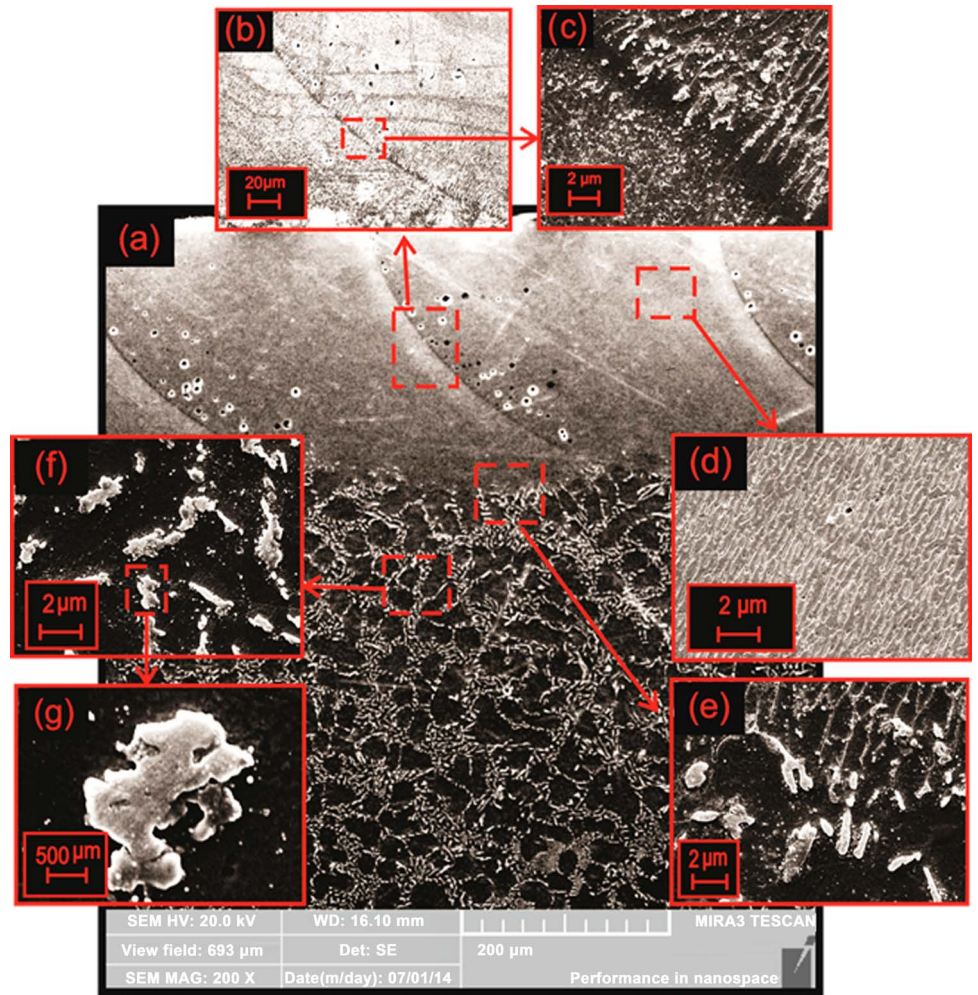
Figure 1. SEM image of the cross-sections of LSR-treated surface of Al-2.0 wt% Fe alloy. (a) the melted zone and substrate region, (b) the overlapping of consecutive weld fillets, (c) magnified region of the (b), (d) magnified of the laser melted zone, (e) the interface between treated region and the substrate, (f) magnified of the substrate region and (g) higher magnified of the (f).
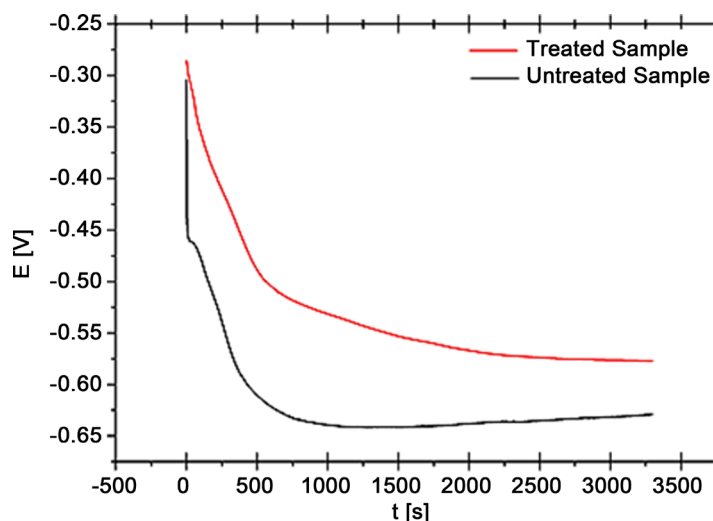
tated on the grain-boundary of the substrate, which may be verified in **Figure 1(a)**. This region has been magnified as such is shown by SEM in **Figure 1**, where it is clearly shown the treated and untreated regions. Moreover, this region was higher magnified as shown in **Figure 1(f)**, where are observed the alloy matrix (green region) and inter-metallic phases (white region) and even with higher magnified can be seen in **Figure 1(g)**, where it is constituted by the intermetallic Al$_3$Fe phase, this results was confirmed by X-ray microanalysis studies (next section).

The characteristic of the melted zone is mainly due to the high cooling rate imposed during RSL-treatment, ASM [13] author asserted, in the low-energy-input laser welding process, it can induce a very high cooling rate (1000 - 10,000 °C·s^{-1}) and laser surface remelting may produce an even higher cooling rate. For this motive, the melted zone can be constituted of metastable phase.

3.3. Low-Angle X-Ray Diffraction (LAXRD) Analysis

The phases formed on the surface of LSR-treated and untreated samples were analyzed

using LAXRD technique, as described in the Materials and Methods section.

LAXRD analysis revealed the presence of Al_2O_3 and AlN phases in most of the diffraction peaks of the treated sample (see **Figure 2**). This figure shows the diffraction peaks of the untreated and treated samples. As can be seen, the intensity of the diffraction peaks of the treated sample is higher than the untreated sample, this may be due to the presence of the new phase, among them AlN phase, which is consistent with the findings reported by Bian *et al*. [14] and Pariona [8].

In this study, the high energy applied in the laser-treatment, allied to the fact that it was carried out in a suitable environment, for the formation of oxides and nitrides, favored the characteristics of high hardness, wear and corrosion resistance of the samples LSR-treated in acidic or alkaline media, as has also been reported by Patnaik [15].

In addition to the simple metal phases shown in **Figure 2**, intermetallic metastable phases were also identified, such as, AlFe, $AlFe_3$ and $Al_{13}Fe_4$. The formation of these phases is important because they determine the roughness, hardness and corrosion behavior of the treated layer. Other authors have also made this type of analysis, among them, Bertelli *et al*. [12], Pariona *et al*. [8], and Gremaud *et al*. [16].

3.4. Corrosion behavior

3.4.1. The Polarization Resistance of Laser-Treated and Untreated Samples

Figure 3 shows the current density behavior, after a linear polarization ± 10 mV around of the corrosion potential of Al-2.0 wt% Fe alloys, for LSR-treated and untreated samples, where the red line represents the results for the treated sample, while, the dark color curve is to the substrate without treatment.

The micropolarization of ±10 mV around corrosion potential promotes a perturbation in the equilibrium potential, giving the appearance of an anodic and cathodic current in the electrochemical cell circuit. This technique of electric current versus applied

Figure 2. LAXRD profiles on the surface treatment of Al-2.0 wt% Fe alloy sample.

Figure 3. Linear Polarization near of the Ecorr for studied electrodes of Al-2.0 wt% Fe alloys versus ECS in 0.1 mol/L H_2SO_4 at 25˚C.

potential was conducted to the laser-treated and untreated samples, and the result is shown in **Figure 3**. The inverse slope of the line in **Figure 3** allows to determine the polarization resistance of the system, that is associated with the charge transfer processes in the interface metal/oxide/electrolyte solution. Therefore, the laser-treated microstructure characteristic definitely influences the polarization resistance (Rp) in relation to untreated substrate. The inverse of the slope of **Figure 3** allowed determined the Rp for both types electrodes, according to the analysis, one can see that the line corresponding to the substrate has a slope greater than the laser-treated sample, ie, at the substrate can be perceived that the current density suffers a greater variation, consequently generates a lower R_p for the substrate. The data obtained confirm this fact, for the laser-treated sample was determined, the R_P equal a 22.1 K ohms, however, for the substrate was 2.08 K ohms, which means an increase of about 11 times R_p for the laser-treated sample relative to the untreated sample, this result showed that the metal/solution interface has different behavior and consequently the polarization resistance has direct impact on the corrosion rates of these surfaces in sulfuric acid. Second Li *et al.* [17], the highest polarization resistance of the treated sample is related to the greater difficulty of charge transfer at the interface between the electrode and the electrolyte solution, possibly indicating the formation of new phases in the treated surface, implying directly on the corrosion resistance of the material. Also, a similar result for Al-1.5 wt% Fe alloy was widely discussed by the authors Pariona *et al.* [8] and Peyre *et al.* [18] discussed a similar result for 316 L steel.

### 3.4.2. Corrosion Resistance, Tafel Plots for LSR-Treated and Untreated Alloy
Figure 4 shows the open-circuit corrosion potentials of the laser-treated surface of the as-received Al-2.0 wt% Fe sample and of the substrate. The open circuit potential was recorded continuously for 1 h after immersion using a saturated calomel (SC) reference electrode. In **Figure 4** it is noted that potential corrosion, which to decrease as a function of time, being more evident for the substrate, around 700 s the substrate reaches stability and after 2000 s the potential tends to increase slightly. However, the LSR-

treated sample decreases more slowly when the time increases, and after 2000 s the regrowth is slower still. For longer times can predict and that these potentials can be find. Comparing the two curves (Figure 4), the corrosion potential of the LSR-treated alloy was increased by up to 8 mV, after 1 h in relation to the untreated material, which can be noticed in this figure. Therefore, the laser-treated alloy became nobler than the untreated one. A similar result to this work was discussed by the authors Khalfaoui *et al.* [19]. These same authors have also shown, when the laser-treated and untreated samples were exposed in a corrosive solution for 2 h, several corrosion pits were observed in the untreated surface while the laser-treated layer was unaltered. This proves that the sample LSR-treated is more resistant to corrosion than the untreated sample. Also the authors Pariona *et al.* [8] showed a similar study to this research for Al-1.5 wt% Fe alloy.

The anodic polarization curves are shown in Figure 5, where a comparison was made between the curves obtained from LSR-treated and untreated alloy, in order to analyses the effects of LSR-treated on the corrosion resistance.
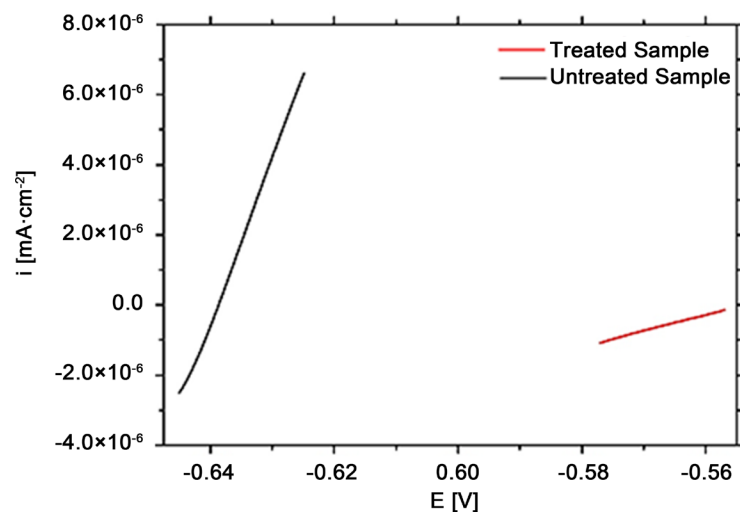
Figure 4. Evolution of open-circuit potential of the Al-2.0 wt% Fe alloy for LSR-treated and untreated samples, during immersion in 0.1 mol/L of H_2SO_4 to 25°C.
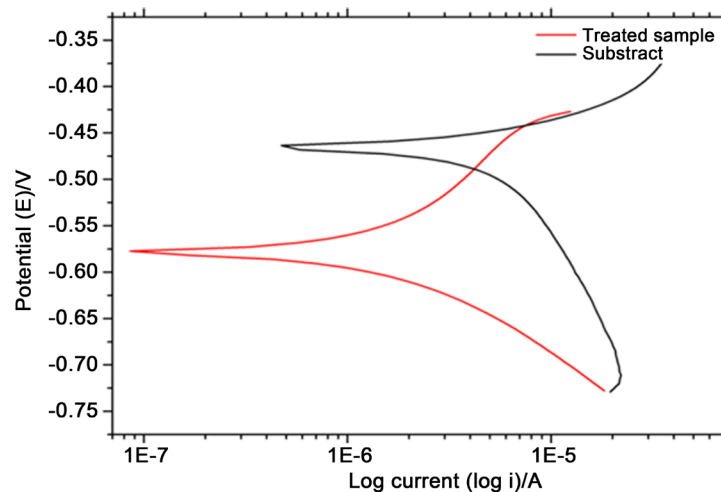
Figure 5. Effect of LSR-treated and untreated alloy under the application of Tafel plots during immersion in 0.1 mol/L of H_2SO_4 to 25°C.

Figure 5 shows the results of the electrochemical polarization measurements of the laser-treated and untreated specimens. At open circuit potential (Ecorr), the corrosion current density ($i$corr) of the untreated and laser-treated specimens was calculated, equal to 9.73×10^{-7} A/cm^2 and 9.95×10^{-6} A/cm^2, respectively. This means in ten-fold decrease the corrosion current for the laser-treatment sample. This fact can be considered due to the presence of Al_2O_3 and AlN phases, in most of the diffraction peaks of the treated sample (see **Figure 2**).

As a consequence of the application of the open-circuit corrosion potentials, linear micropolarization and of the anodic polarization curves and the result is summarized in **Table 1**, where are shown the electrochemical parameters for Al-2.0 wt% Fe alloy for LSR-treated and untreated samples. Where, Ecorr is the open circuit potential, Rp is the polarization resistance, β_A and β_C anodic and cathodic Tafel constants, and I_{corr} is the corrosion current density. According to the result of **Table 1**, the electrochemical parameters that correspond to the material LSR-treated showed better results than the untreated material.

3.4.3. Cyclic Voltammetry Technique

Electrochemical methods make use of measurable electrical properties (current electrical, potential differences, accumulation interfacial charge, among others), from phenomena in which a redox species interacts, physically and/or chemically with other components of the medium, or even with interfaces. Luther *et al.* [20] pointed out, that the efficiency of cyclic voltammetry technique, result of its feature to provide rapid information on the thermodynamics of redox processes, of the heterogeneous reaction kinetics of electron transfer and on chemical reactions coupled to adsorptive processes. Yet these same authors argue that, there are two main components, which determine the reactions, which occur in the electrode: diffusional mass transfer of the analytic in solution to the electrode surface, and heterogeneous charge transfer between the analytic and the electrode. In some cases may occur chemical reactions coupled to any of these processes. Yet they affirm, Butler-Volmer equation is the basic equation of the electrochemical kinetics, which expressed these relationships.

A comparative study was carried out of the cyclic polarization to the laser-treated and untreated samples, with the purpose of studying the behavior of these materials in the same electrolyte solution. **Figure 6** shows the comparison between the cyclic polarizations curves for the laser-treated and untreated specimens, in aerated solution of H_2SO_4 0.1 mol·L^{-1}, at 25°C. The oxidation peaks and the reduction peaks are no observed in both samples in the potential range shown in **Figure 6**, demonstrating that

Table 1. Electrochemical parameters obtained for Al-2.0 wt% Fe alloy for LSR-treated and untreated samples in 0.1 mol/L H_2SO_4 performed by technical open-circuit corrosion potentials, linear micropolarization and anodic polarization curves.

Region	Ecorr (V)	R_p (KΩ)	β_a (V/dec)	β_c (V/dec)	Icorr (A/cm^2)	Corrosion rate (mm/year)
Treated Surface	−0.577	22.1	0,.086	0.117	9.37e−7	0.07
Untreated Substrate	−0.629	2.08	0.066	0.172	9.95e−6	0.78
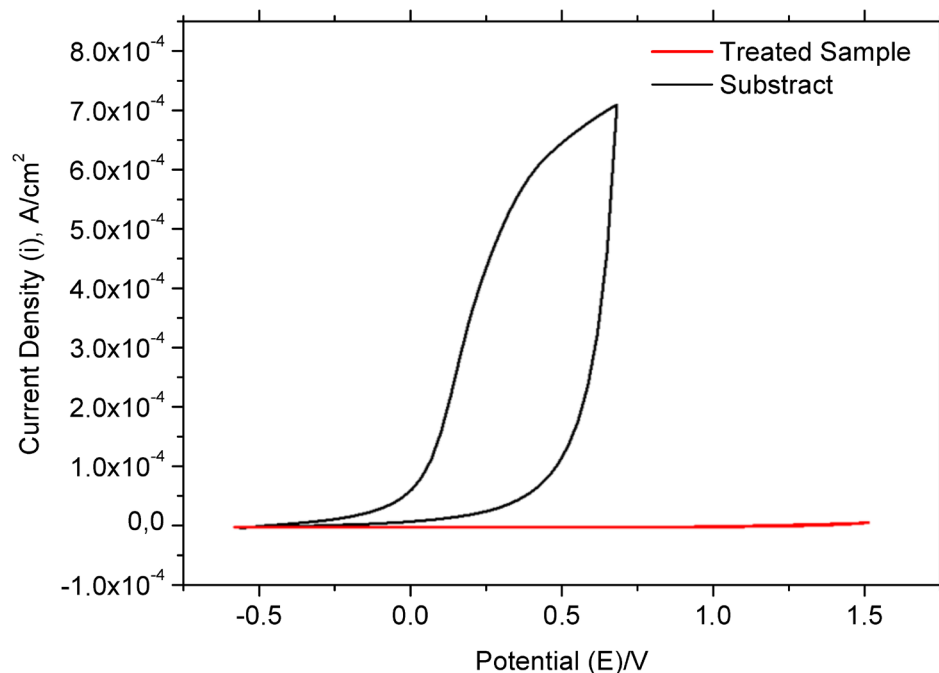
Figure 6. Cyclic voltammograms for the LSR-treated and untreated samples.

these reactions are of irreversible character at this condition.

The cyclic polarizations for the untreated specimen in H_2SO_4 aerated solution is shown in **Figure 6** (black line). The cycle starts in −1.0 V until the most anodic value +0.70 V, where in this potential the current density is about 6.5×10^{-4} A/cm^2, versus SCE, returning to −1.0 V, however the current density has a steady behavior, with low current density for the sample LSR-treated in the same potential range. For untreated sample, during the anodic scan, there is a current increase near the −0.10 V, associated with the dissolution of aluminum, followed by the formation of an aluminum oxide (Al_2O_3) film on the sanded substrate. The anodic current rapidly increased until approximately +0.30 V, followed by a smaller growth rate until +0.70 V; it is characterized as a region of thickening of the oxide film. According to the authors Kikuchi *et al.* [21], the potential increased linearly with anodizing time, due to the formation of a barrier anodic oxide film, via the following electrochemical reaction,

$$2Al + 3H_2O = Al_2O_3 + 6H^+ + 6e^-$$

With the linear increase in the potential, the thickness of the barrier layer increased with anodizing time; in other words, the thickness increased with anodizing potential. After the inversion potential, there is a sharp drop of the anodic current up to +0.50 V and, thereafter, reaching low values of currents in potential close to 0.0 V.

The cyclic polarization curve of **Figure 6** (line red), it corresponds to the laser-treated sample. The anodic current increases from potential +0.5 V as can be appreciated, this can be associated with the growth of the aluminum oxide film and/or Al-Fe phases on the laser-treated surface, which is constituted by different phases, such as Al_2O_3, AlFe, $AlFe_3$ and $Al_{13}Fe_4$ and AlN, this was confirmed by X-ray (**Figure 2**). In the cyclic polarization curve, the cycle starts in −1.0 V until the most anodic value +1.6 V, where the current density is about 0.2×10^{-6} A/cm^2 in +0.7 V. This result mean in 0.7

V, the current density which corresponds to the LSR-treated sample is much lower than untreated sample, being around 3 times.

According to this result, the LSR-treated sample showed clearly the passive zone. However, the LSR-treated sample results in reduction of the current density, and this fact indicates a lower corrosion rate and therefore it takes an improvement in the corrosion resistance, this fact can be verified, otherwise, the corrosion rate according to Table 1 was reduced by 11 times for the LSR-treated sample, compared to the untreated sample. According to the previous discussion, the surface of LSR-treated sample was modify drastically, therefore the electrochemical corrosion behavior in 0.1 mol/L H_2SO_4 was propitiate the passivity on the surface of LSR-treated sample, reducing so the corrosion phenomena.

4. Conclusions

According to this study, the following conclusions were made, then:

1) The melted zone is mainly due to high cooling rate imposed during RSL-treatment sample;

2) Therefore, the melted zone was constituted of metastable phases and by LAXRD analysis revealed the presence mainly of Al_2O_3 and AlN phases;

3) These phases contributed in the microstructural modification, favored the characteristics of high hardness and corrosion resistance of the LSR-treated sample in sulfuric acidic;

4) The polarization resistance has been increased about 11 times for the laser-treated sample relative to the untreated sample, implying directly on the corrosion resistance of the material;

5) In result of the electrochemical study, it was also observed, in ten-fold decrease, the corrosion current after the laser-treatment had occurred;

6) In the technique of cyclic voltammograms, the reduction and (re)oxidation reverse peaks/waves were not observed in both samples in the same potential range and so demonstrating that these reactions are of irreversible character at this condition;

7) The LSR-treated sample showed clearly a wide passive zone. However, the LSR-treated sample results in reduction of the current density, and this fact indicates a lower corrosion rate and therefore it acts in improvement in the corrosion resistance;

8) The electrochemical parameters that correspond to the LSR-treated material showed better results than the untreated material. Therefore, this type of laser-treated alloy can be applied in the aerospace, aeronautic and automobilist industries;

9) To better understand the efficiency of the treated material laser, other studies are being carried out, such as, microhardness, study of the roughness by atomic force technique, electrochemical impedance spectroscopy, Raman spectroscopy and numerical simulation by finite element using the Marangoni phenomenon and optimized by Multigrid technique.

Acknowledgements

References

[1] Nakajima, D., Kikuchi, T., Natsui, S., Sakaguchi, N. and Suzuki, R.O. (2015) Fabrication of a Novel Aluminum Surface Covered by Numerous High-Aspect-Ratio Anodic Alumina Nanofibers. *Applied Surface Science*, **356**, 54-62. https://doi.org/10.1016/j.apsusc.2015.08.030

[2] Lee, S.-J., Park, C., Lim, Y.-S. and Kwon, H.-S. (2003) Influences of Laser Surface Alloying with Niobium (Nb) on the Corrosion Resistance of Zircaloy-4. *Journal of Nuclear Materials*, **321**, 177-183. https://doi.org/10.1016/S0022-3115(03)00245-9

[3] Riva, R., Lima, M.S.F., Rodrigues, N.A.S. and Cardoso, J.C.M. (2007) Using an Ytterbium Fiber Laser to Fracture Splitting of Compacted Graphite Iron Bearing Caps. *Proceedings of the Fourth International WLT-Conference on Lasers in Manufacturing*, Munich, June 2007, 65-70.

[4] Steen, W.M. and Mazumder, J. (2010) Laser Material Processing. 4th Edition, Springer, New York. https://doi.org/10.1007/978-1-84996-062-5

[5] Pariona, M.M., Teleginski, V., dos Santos, K., Machado, S., Zara, A.J. and Zurba, N.K. (2012) Yb-Fiber Laser Beam Effects on the Surface Modification of Al Fe Aerospace Alloy Obtaining Weld Filet Structures, Low Fine Porosity and Corrosion Resistance. *Surface Coating Technology*, **206**, 2293-2301. https://doi.org/10.1016/j.surfcoat.2011.10.007

[6] Pariona, M.M., Teleginski, V., dos Santos, K., dos Santos, E.L.R., de Lima, A.C., Zara, A.J. and Riva, R. (2012) AFM Study of the Effects of Laser Surface Remelting on the Morphology of Al-Fe Aerospace Alloys. *Materials Characterization*, **276**, 64-76. https://doi.org/10.1016/j.matchar.2012.08.011

[7] Sun, Z., Annergren, I., Pan, D. and Mai, T.A. (2013) Effect of Laser Surface Remelting on the Corrosion Behavior of Commercially Pure Titanium Sheet. *Materials Science and Engineering: A*, **345**, 293-300. https://doi.org/10.1016/S0921-5093(02)00477-X

[8] Pariona, M.M., Teleginski, V., dos Santos, K., de Lima, A.A.O.C., Zara, A.J., Micene, T.M. and Riva, R. (2013) Influence of Laser Surface Treated on the Characterization and Corrosion Behavior of Al-Fe Aerospace Alloys. *Applied Surface Science*, **276**, 76-85. https://doi.org/10.1016/j.apsusc.2013.03.025

[9] Yan, C., Hao, L., Hussein, A., Young, P., Huang, J. and Zhu, W. (2015) Microstructure and Mechanical Properties of Aluminium Alloy Cellular Lattice Structures Manufactured by Direct Metal Laser Sintering. *Materials Science & Engineering: A*, **628**, 238-246. https://doi.org/10.1016/j.msea.2015.01.063

[10] Olakanmia, E.O., Cochranea, R.F. and Dalgarno, K.W. (2015) A Review on Selective Laser Sintering/Melting (SLS/SLM) of Aluminium Alloy Powders: Processing, Microstructure, and Properties. *Progress in Material Science*, **74**, 401-477. https://doi.org/10.1016/j.pmatsci.2015.03.002

[11] Fu, B., Qin, G., Meng, X., Ji, Y., Zou, Y. and Lei, Z. (2014) Microstructure and Mechanical Properties of Newly Developed Aluminum-Lithium Alloy 2A97 Welded by Fiber Laser. *Materials Science & Engineering: A*, **617**, 1-11. https://doi.org/10.1016/j.msea.2014.08.038

[12] Bertelli, F., Meza, E.S., Goulart, P.R., Cheung, N., Riva, R. and Garcia, A. (2011) Laser Remelting of Al-1.5 wt% Fe Alloy Surfaces: Numerical and Experimental Analyses. *Optics and Lasers in Engineering*, **49**, 490-497. https://doi.org/10.1016/j.optlaseng.2011.01.007

[13] ASM Handbook (1993) Welding, Brazing and Soldering. Vol. 6, ASM International, Materials Park, OH.

[14] Bian, H.-M., Yang, Y., Wang, Y., Tian, W., Jiang, H.-F., Hu, Z.-J. and Yu, W.-M. (2012) Alumina-Titania Ceramics Prepared by Microwave Sintering and Conventional Pressure-Less Sintering. *Journal of Alloys and Compounds*, **525**, 63-67. https://doi.org/10.1016/j.jallcom.2012.02.071

[15] Patnaik, P. (2001) Handbook of Inorganic Chemicals. McGraw-Hill, Burlington.

[16] Gremaud, M., Carrard, M. and Kurz, W. (1990) The Microstructure of Rapidly Solidified Al-Fe Alloys Subjected to Laser Surface Treatment. *Acta Metallurgia et Materialia*, **38**, 2587-2599. https://doi.org/10.1016/0956-7151(90)90271-H

[17] Li, C., Wang, Y., Guo, L., He, J., Pan, Z. and Wang, L. (2010) Laser Remelting of Plasma-Sprayed Conventional and Nanostructured Al2O3-13 wt% TiO2 Coatings on Titanium Alloy. *Journal of Alloys and Compounds*, **506**, 356-363. https://doi.org/10.1016/j.jallcom.2010.06.207

[18] Peyre, P., Scherpereel, X., Berthe, L., Carboni, C., Fabbro, R., Be'ranger, G. and Lemaitre, C. (2000) Surface Modifications Induced in 316L Steel by Laser Peening and Shot-Peening. Influence on Pitting Corrosion Resistance. *Materials Science and Engineering*: A, **280**, 294-302. https://doi.org/10.1016/S0921-5093(99)00698-X

[19] Khalfaoui, W., Valerio, V., Masse, J.E. and Autric, M. (2010) Excimer Laser Treatment of ZE41 Magnesium Alloy for Corrosion Resistance and Microhardness Improvement. *Optics and Lasers in Engineering*, **48**, 926-931. https://doi.org/10.1016/j.optlaseng.2010.03.009

[20] Luther, G.W., Glazer, B.T., Ma, S., Trouwborst, R.E. and Moore, T.S. (2008) Use of Voltammetric Solid-State (Micro)Electrodes for Studying Biogeochemical Processes: Laboratory Measurements to Real Time Measurements with an *in Situ* Electrochemical Analyzer (ISEA). *Marine Chemistry*, **108**, 221-235. https://doi.org/10.1016/j.marchem.2007.03.002

[21] Kikuchi, T., Nakajima, D., Kawashima, J., Natsui, S. and Suzuki, R.O. (2014) Fabrication of Anodic Porous Alumina via Anodizing in Cyclic Oxocarbon Acids. *Applied Surface Science*, **313**, 276-285. https://doi.org/10.1016/j.apsusc.2014.05.204